Journal of Alloys and Compounds 509 (2011) 2160–2163

Contents lists available at ScienceDirect

Journal of Alloys and Compounds

journal homepage: www.elsevier.com/locate/jallcom

Synthesis and characterization of nanocrystalline Ti-substituted Zn ferrite

P.P. Hankare[a,*], R.P. Patil[a,*], A.V. Jadhav[a], R.S. Pandav[a], K.M. Garadkar[a], R. Sasikala[b], A.K. Tripathi[b]

[a] Department of Chemistry, Shivaji University, Kolhapur 416004, Maharashtra, India
[b] Chemistry Division, Bhabha Atomic Research Center, Mumbai 400085, Maharashtra, India

ARTICLE INFO

Article history:
Received 22 April 2010
Received in revised form 25 October 2010
Accepted 28 October 2010
Available online 9 November 2010

Keywords:
Ferrite
Sol–gel synthesis
XRD
FTIR
TEM
EDAX
VSM

ABSTRACT

Nanocrystalline Ti-substituted zinc ferrite was synthesized by sol–gel autocombustion route. Structural characterization of the sample was carried out by the X-ray diffraction technique which confirms that it is a single phase cubic ferrite. The FTIR spectra revealed two absorption bands which are attributed to the fundamental vibrational modes of tetrahedral and octahedral complexes of the unit cell. The IR bands due to tetrahedral complexes are found to shift slightly towards higher frequency side where as that due to octahedral complexes are found to shift towards lower frequency side. The particle size of the Ti-substituted zinc ferrite was estimated to be ~30 nm. The elemental analysis as obtained from EDAX is in close agreement with the starting composition used for the synthesis. Vibrating sample magnetometer (VSM) studies indicated that this sample is ferrimagnetic in nature at room temperature.

1. Introduction

The study of metal oxides has attracted the attention of materials researchers due to their optical, electrical, magnetic, mechanical and catalytic properties, which make them technologically useful. The relation between the structure and properties of oxide materials and their applications are of great importance [1–6]. Currently, considerable interest in nanocrystalline oxide materials exists owing to their unusual properties. Decreasing particle size results in some remarkable phenomenon. Unusual optical and electrical properties in these materials take place due to a phenomenon known as quantum confinement [7].

The physicochemical properties of many materials depend on the synthetic methods. Selection of the synthetic route is crucial to control the composition, structure and morphology of a chosen material. A variety of metal-oxides, both simple and complex are prepared by the conventional ceramic method. However, ferrite prepared by such method involves high temperature synthesis for the completion of solid-state reaction between the constituent oxides or carbonates. The particles obtained by this method are rather large and non-uniform in size. These non-uniform particles, on compacting, result in the formation of voids or low density ferrites.

In order to overcome these difficulties, we have studied wet chemical method like sol–gel method to synthesize Ti-doped Zn ferrite nanoparticles. The sol–gel autocombustion method is used to speed up the synthesis of complex materials. It is a simple process, which saves time and energy consumption over the traditional methods and requires only low sintering temperature. This method is employed to obtain ferrites having improved powder characteristics, more homogeneity and narrow particle size distribution [8,9]. To our knowledge, there are no reports on the synthesis and structural property study of the nanocrystalline titanium substituted zinc ferrite, prepared by sol–gel autocombustion method.

2. Experimental details

Polycrystalline sample having the general formula, $ZnTiFeO_4$ was synthesized by sol–gel auto-combustion method. High purity AR grade ferric nitrate, zinc nitrate, titanium isopropoxide and citric acid were used for synthesis. The first step was to synthesize titanium nitrate from titanium isopropoxide using water and nitric acid [7].

$$Ti(i\text{-}OC_3H_7)_4 + 3H_2O \rightarrow TiO(OH)_2 + 4(C_3H_7OH) \quad (1)$$

$$TiO(OH)_2 + HNO_3 \rightarrow TiO(NO_3)_2 + 2H_2O \quad (2)$$

The metal nitrate solutions were mixed in the required stoichiometric ratios in distilled water. The pH of the solution was maintained between 9 and 9.5 using ammonia solution. The solution mixture was slowly heated around 373 K with constant stirring to obtain a fluffy mass. This precursor powder was sintered at 973 K for 8 h. The flow chart of this procedure is given below. For making the pellets, the powder was mixed with 2% polyvinyl alcohol (binder) and pressed uniaxially at a pressure of 8 ton/cm^2.

The phase formation of the samples was confirmed by X-ray diffraction studies using Philips PW-1710 X-ray diffractometer with CrKα radiation (λ = 2.2897 Å). The

* Corresponding authors. Tel.: +91 231 2609381.
E-mail addresses: p_hankarep@rediffmail.com (P.P. Hankare), raj_rbm_raj@yahoo.co.in (R.P. Patil).

0925-8388/$ – see front matter © 2010 Elsevier B.V. All rights reserved.
doi:10.1016/j.jallcom.2010.10.173

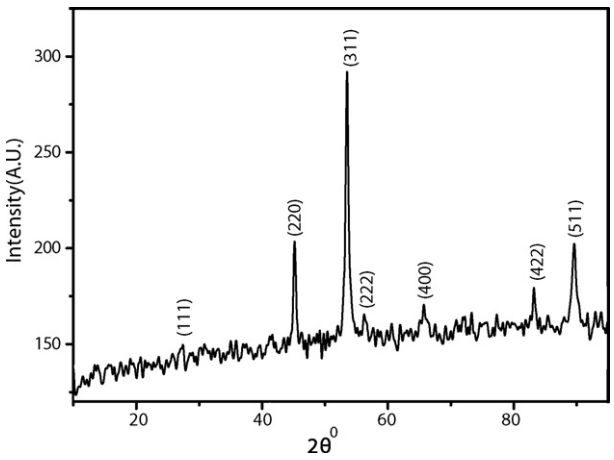

Fig. 1. X-ray diffraction pattern of $ZnTiFeO_4$.

lattice parameter was calculated for the cubic phase using following relation [10].

$$\frac{1}{d^2} = h^2 + k^2 + \frac{l^2}{a^2} \quad (3)$$

From the X-ray diffraction peaks, crystallite size was estimated using Scherrer's formula.

$$t = \frac{0.9\lambda}{\beta \cos\theta} \quad (4)$$

where symbols have their usual meaning.

The particle density was calculated according to the formula $dx = 8M/Na^3$, where M is the molecular mass, N is the Avogadro's number, and a is the lattice parameter which was calculated from the X-ray diffraction pattern. The FTIR spectra were recorded in a Perkin Elmer FTIR spectrometer using KBr pellets. The surface morphology and particle size of the ferrite sample were studied by using PHILIPS, CM200 (operating voltages: 20–200 kV) transmission electron microscope (TEM). Elemental analysis was done using EDAX (SEM: EDAX Model JEOL-JSM6360) spectroscopy. The magnetic property of the sample was studied by vibrating sample magnetometer (VSM).

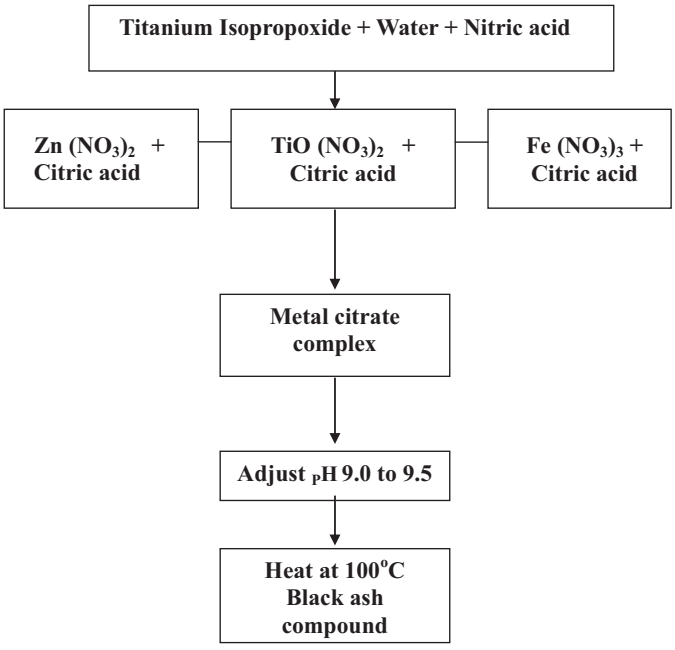

3. Results and discussion

3.1. Phase identification

X-ray diffraction pattern of titanium substituted zinc ferrite powder is shown in Fig. 1. The diffraction pattern indicates that it is a single phase crystalline compound and the peak positions match well with the standard data of zinc ferrite (JCPDS Card No. 35-1373). The crystallite size calculated from the width of the XRD peak is around 30 nm. The values of lattice constant (a), crystallite size (t) and X-ray density (dx) for this sample are given in Table 1.

Table 1
Data on lattice parameter, crystallite size, X-ray density of $ZnTiFeO_4$ ferrite sample.

Composition	Lattice constant (a), Å	Crystallite size (t), nm	X-ray density (dx), g/cm^3
$ZnTiFeO_4$	8.432	30.0	4.75

3.2. FTIR spectrum

From, FTIR spectra were recorded to confirm the formation of nanocrystalline spinel $ZnTiFeO_4$. We have studied the effect of sintering temperature 373–973 K on infra-red spectra of the sample in the range of 350–2500 cm^{-1} is shown in Fig. 2. In FTIR spectroscopy of metal oxides, we consider two ranges of the absorption bands, 350–450 and 500–650 cm^{-1} as suggested by previous work [11,12]. The intensive broadband at 1620 cm^{-1} is due to O–H stretching vibration interacting through hydrogen bonds. Traces of adsorbed CO_2 are evidenced by the very small absorption peak around 2340 cm^{-1}. The ν (C=O) stretching vibration of the carboxylate group (CO^{2-}) is observed around 1380 cm^{-1} and the band at ~1090 cm^{-1} corresponds to nitrate ions traces. Therefore, the CO^{3-} and CO^{2-} vibrations disappeared when calcination temperature was increased. In the range of 1000–350 cm^{-1}, two main metal–oxygen bands at ~552 cm^{-1} and 418 cm^{-1} were observed for the sample calcined at 973 K. The high frequency band 552 cm^{-1} is due to the vibration of the tetrahedral M···O bond and the low frequency band 418 cm^{-1} is due to the vibration of the octahedral M···O bond in the crystal lattices of the $ZnTiFeO_4$ sample.

3.3. Transmission electron micrograph study

Fig. 3(a) depicts transmission electron micrograph (TEM) of $ZnTiFeO_4$ sample. The corresponding selected area electron diffrac-

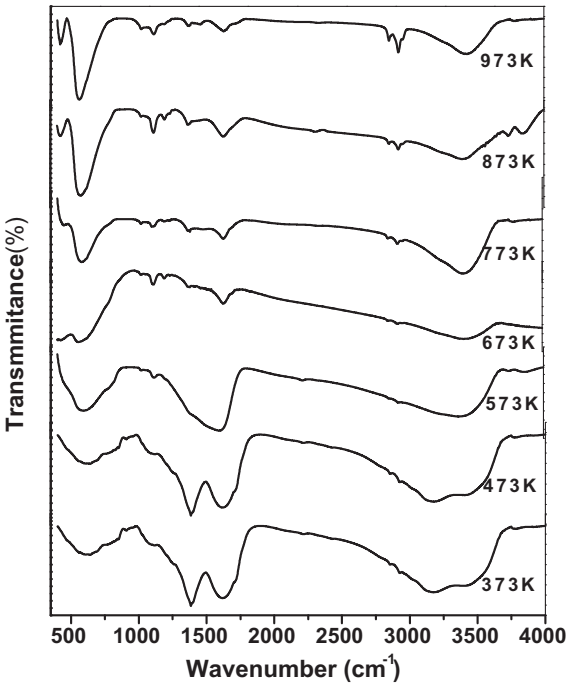

Fig. 2. FTIR spectra of $ZnTiFeO_4$ composition with different sintering temperature.

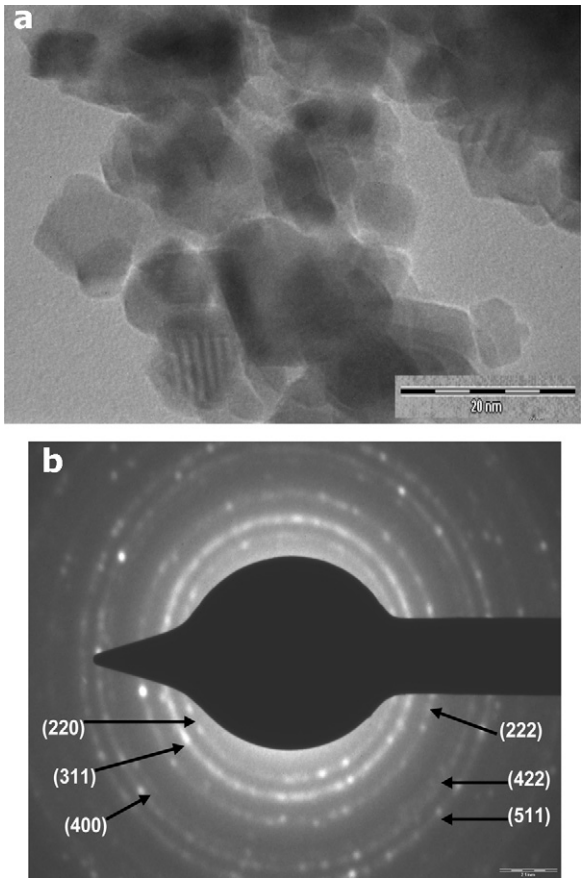

Fig. 3. (a) Transmission electron microscopy for the $ZnTiFeO_4$. (b) SAED pattern for the $ZnTiFeO_4$.

togram (SAED) is given in Fig. 3(b). It is evident from these micrographs that all the synthesized sample have particle size ranging from 25 to 30 nm. This is in close agreement with the crystallite size obtained from the XRD pattern (Table 1). The superimposition of the bright spot with Debye ring pattern indicates polycrystalline nature of the sample. The SAED pattern of this sample also confirms the single phase formation of $ZnTiFeO_4$.

Table 2
Atomic percentage value for the $ZnTiFeO_4$ sample by EDAX analysis.

Composition (x)	Atomic % for element					
	Zn		Ti		Fe	
	Expt.	Thero.	Expt.	Thero	Expt.	Thero.
$ZnTiFeO_4$	34.93	33.33	28.98	33.33	36.09	33.33

3.4. Energy dispersion X-ray analysis

The composition of the nanocrystalline metal oxide has been determined using the energy dispersion X-ray analysis (EDAX). The X-ray analysis spectrum of $ZnTiFeO_4$ is shown in Fig. 4. From the EDAX spectrum, the presence of Zn, Ti, Fe and O are confirmed in this sample. The quantitative analysis of EDAX spectrum revealed the relative atomic ratio of Zn:Ti:Fe of about 1:1:1, which are close to the expected values for $ZnTiFeO_4$. The data of the EDAX analysis for this sample is given in Table 2.

3.5. Magnetic study

Magnetic properties of this sample was carried out by using vibrating sample magnetometer (VSM) and it is depicted in Fig. 5. This sample shows a typical S-type shape in M–H curve, though the coercive force is very small. The magnetization rises very sharply as the applied field increases from zero in either direction and then slowly approaches saturation. This is the typical behavior of nanosized magnetic material where residual superparamagnetic relaxation leads to slow rise in the wings and ferrimagnetic part contributes to hysteresis loop with small coercive field. In zinc ferrite the magnetization appears due to cationic inversion at smaller particle size. Thus as the particles size increases, the inversion decreases and the magnetization decreases. The magnetic data for the samples reveals that, it is ferrimagnetic in nature.

4. Conclusions

Nanocrystalline particles of $ZnTiFeO_4$ were successfully synthesized by the sol–gel autocombustion route. The X-ray diffraction study reveals the formation of cubic spinel structure. FTIR spectra exhibited two main metal–oxygen bands at ~552 cm^{-1} and 418 cm^{-1} corresponding to the vibration of the tetrahedral and

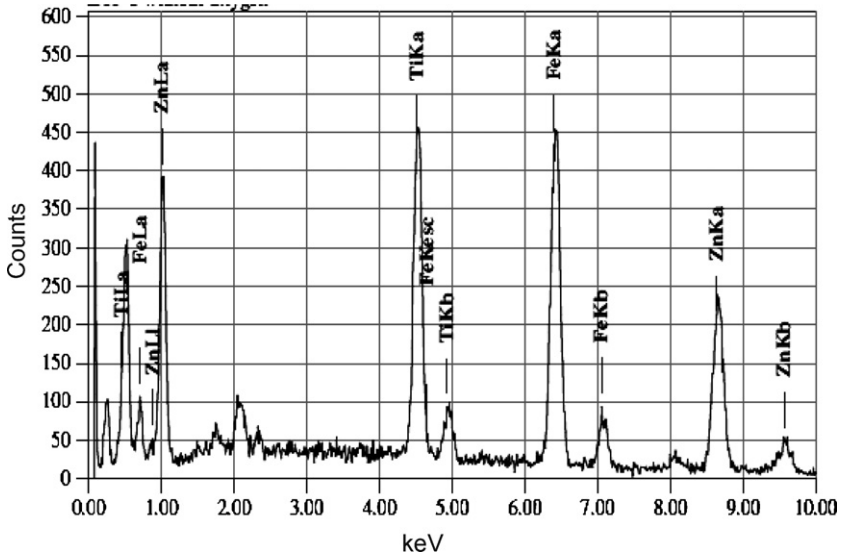

Fig. 4. Energy X-ray dispersive spectrum for $ZnTiFeO_4$.

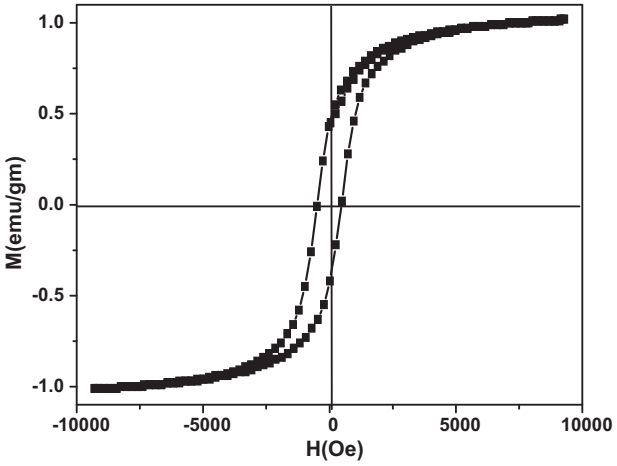

Fig. 5. Vibrating sample magnetometer loop (VSM) for $ZnTiFeO_4$.

octahedral M···O bond respectively, confirming the formation of spinel $ZnTiFeO_4$. Particle size of this sample was estimated to be ~30 nm. Magnetic study shows that $ZnTiFeO_4$ is strongly ferrimagnetic in nature.

Acknowledgement

Author (PPH) is very thankful to DAE-BRNS, Mumbai for financial assistance through Major research project No. 2009/37/41/BRNS/2231.

References

[1] G. Blasse, Philips Res. Rep. (Netherlands) 20 (1965) 528.
[2] J.B. Goodenough, Magnetism and the Chemical Bond, John Wiley, New York, 1966.
[3] J.B. Goodenough, A.L. Loeb, Phys. Rev. 98 (1955) 391.
[4] A.P.B. Sinha, N.R. Sanjana, A.B. Biswas, Acta Cryst. 10 (1957) 439.
[5] P. Nathawani, V.S. Darshane, J. Phys. C (Solid State Phys.) 2 (1988) 3191.
[6] K.H.J. Buschow, Handbook of Magnetic Materials, 8, Elsevier, Amsterdam, 1995.
[7] K.C. Patil, M.S. Hegde, Tanu Rattan, S.T. Aruna, Chemistry of Nanocrystalline Oxide Materials. World Scientific Publishing, 2008, p. 3.
[8] P.P. Hankare, R.P. Patil, U.B. Sankpal, S.D. Jadhav, P.D. Lokhande, K.M. Jadhav, R. Sasikala, J. Solid State Chem. 182 (2009) 3217.
[9] P.P. Hankare, R.P. Patil, U.B. Sankpal, K.M. Garadkar, R. Sasikala, A.K. Tripathi, I.S. Mulla, J. Magn. Magn. Mater. 322 (2010) 2629.
[10] B.D. Cullity, Elements of X-ray Diffraction, Addison-Wesley Publishing, Reading, MA, 1956, p. 352.
[11] A.D. Sheikh, V.L. Mathe, J. Mater. Sci. 43 (2008) 2018.
[12] R.D. Waldron, Phys. Rev. 99 (1955) 1727.